第 34 卷第 9 期
2018 年 9 月

无 机 化 学 学 报
CHINESE JOURNAL OF INORGANIC CHEMISTRY

Vol.34 No.9
1701-1709

一种简单的提高无定形 TiO_2 光催化活性的方法及其在增透膜中的应用

李远洋[1] 晏良宏*,[2] 江 波*,[1]

([1]四川大学化学学院绿色化学与技术教育部重点实验室,成都 610064)

([2]中国工程物理研究院激光聚变研究中心,绵阳 621900)

摘要:通过简单的溶胶–凝胶法制备得到了小粒径的无定形 TiO_2 粒子,并将其沉积在多孔 SiO_2 膜层表面,多孔 SiO_2 膜层大的表面积有助于无定形 TiO_2 的良好分散,高度分散的无定形 TiO_2 粒子对膜层的光学性能影响较小,通过匹配合适的低折射率的 SiO_2 膜层,制备得到的 SiO_2& 无定形 TiO_2 (SiO_2&amorphous-TiO_2) 膜层表现出和理想单层增透膜相似的光学性能。同时 SiO_2&amorphous-TiO_2 的光催化性能显著提高,明显高于单层无定形 TiO_2。而且 SiO_2& 无定形 TiO_2 膜层甚至表现出比相应的负载锐钛矿型 TiO_2 的膜层,即 SiO_2& 锐钛矿 TiO_2,更高的光催化活性,这一反常现象的原因是,无定型 TiO_2 膜层表面丰富的羟基有助于减少空穴–电子对的复合,其相对疏松的结构能够加快光生电子–空穴的转移速率,而这些因素的影响超过了晶型结构对光催化活性的影响。同时 SiO_2 膜层的孔隙结构在浸渍–提拉镀制过程中,自发形成并不需要后续热处理过程,因此,整个 SiO_2& 无定形 TiO_2 膜层的制备均可在室温下完成,能够实现其在不耐热基片上的应用。

关键词:溶胶–凝胶; 无定形 TiO_2; SiO_2; 薄膜; 防反射; 光催化

中图分类号:O612.4 **文献标识码**:A **文章编号**:1001-4861(2018)09-1701-09

DOI:10.11862/CJIC.2018.205

Simple Way to Enhance the Photocatalytic Activity and Application in Antireflective Coatings for Amorphous TiO_2

LI Yuan-Yang[1] YAN Liang-Hong*,[2] JIANG Bo*,[1]

([1]*Key Laboratory of Green Chemistry & Technology, College of Chemistry, Sichuan University, Chengdu* 610064, *China*)

([2]*Research Center of Laser Fusion, China Academy of Engineering Physical, Mianyang, Sichuan* 621900, *China*)

Abstract: Small-sized amorphous TiO_2 nanoparticles were prepared and deposited on mesoporous SiO_2 support via sol-gel method at room temperature. This structure greatly increases the surface areas of the amorphous TiO_2 particles, which facilitates the enhancement of photocatalytic activity and preserved the optical performance of the films in the same time. The resultant SiO_2&amorphous-TiO_2 films afford glasses a maximum transmittance of 99.97% and show a much higher photocatalytic activity than the monolayer amorphous TiO_2 film. Surprisingly, the SiO_2&amorphous-TiO_2 even shows a higher photocatalytic activity than the counterparts with anatase phase. This higher photocatalytic activity is attributed to abundant surface hydroxyl groups and relative loose structure of the amorphous TiO_2 nanoparticles, which can help enhance photocatalytic activity through reducing recombination of electron-hole pairs and increase the migration rates of the photoexcited electrons and holes, respectively. And these characteristics may be preferable to crystal structure for enhancing photocatalytic activity. Meanwhile, the coating process is very simple, low cost and conducted at room temperature, which is feasible for polymer substrates.

Keywords: sol-gel process; amorphous titanates; silicates; thin films; antireflection; photocatalysis

收稿日期:2018-03-22。收修改稿日期:2018-06-12。

国家自然科学基金(No.)资助项目。

*通信联系人。E-mail:yanlianghong@126.com,jiangbo@scu.edu.cn

0 Introduction

TiO_2-based coatings can be applied easily on transparent substrates such as glass and plastics to provide self-cleaning function. However, the TiO_2 coatings developed thus far always enhance the surface reflection of transparent substrates due to the high refractive index (n>2)[1]. To meet the conflicting requirements of antireflection (AR) and self-cleaning function, an effective way is to apply a low-refractive-index material such as SiO_2 into TiO_2 coatings. Common practices include: (i) the preparations of the TiO_2 and SiO_2 composite film[2-3], (ii) the design of a double layer structure composed of a SiO_2 bottom layer and a porous/density ultrathin TiO_2 top layer[4-5], (iii) the synthesis of solid/hollow SiO_2&TiO_2 core-shell particles[6-7] and (iv) loading TiO_2-nanoparticles into a highly porous SiO_2 network[8].

However, all these methods realized self-cleaning AR coatings using anatase TiO_2, which will usually need high-temperature treatments to crystallize TiO_2. Or for the studies employed preformed anatase TiO_2 powder, although high temperature treatments can be avoid, the redispersibility of the TiO_2 nanoparticles is also a great challenge. Amorphous TiO_2, which can be prepared at room-temperature, then becomes a better choice to provide AR coatings with self-cleaning function.

It is widely believed that the crystal structure of TiO_2 is the most primitive and essential property to predict photocatalytic activity. And it is commonly considered that amorphous TiO_2 contains high concentrations of defects, which will function as electron-hole recombination centres, and render the amorphous TiO_2 inactive[9-10]. But other physical properties such as surface area[11], particle size[9] and surface hydroxyls[12] also have a great impact on photocatalytic activity of TiO_2. In order to enhance the photoactivity of amorphous titania, extensive efforts have been conducted including constructing special microstructures[11], fabricating hydro-oxygenated amorphous[13-14] and the additives of metal oxides[15].

In our research, a facile, fast and simple method was developed to fabricate self-cleaning AR coatings with amorphous TiO_2 and mesoporous SiO_2. The SiO_2&amorphous-TiO_2 films were prepared by sol-gel dip-coatings method at room temperature. The amorphous TiO_2 nanoparticles with small-size and limited amount were deposited on mesoporous SiO_2 layer. The large surface areas of the mesoporous SiO_2 layer favour dispersion of TiO_2 nanoparticles. This structure greatly increased the surface areas of the amorphous TiO_2 particles, which facilitates the enhancement of photocatalytic activity and preserved the optical performance of the films in the same time.

These SiO_2&amorphous-TiO_2 films exhibit a similar AR function with the ideal single-layer AR coatings. Meanwhile, these films show a great enhancement of photo-catalytic activity compared with the single amorphous TiO_2 layer. Surprisingly, the SiO_2& amorphous-TiO_2 even exhibit a faster photocatalytic degradation rate than the counterparts with anatase phase, *i.e.* SiO_2&anatase-TiO_2. To explain this abnormal finding, the chemical structures of the amorphous and anatase-TiO_2 films were studies. Notably, the mesoporous structure of the SiO_2 coating was spontaneously formed during the sol-gel dip-coating process without the need of post heat treatment. So the entire coating process can be processed at room temperature and the species of the feasible substrate materials can be remarkably expanded.

1 Expermimental

1.1 Materials

Methyltriethoxysilane (MTES) and Tetraethoxysilane (TEOS) were purchased from Alfa Aesar (China) Chemical Co., Ltd. Titanium n-butoxide (n-BuTi, 99%) was purchased from Acros. Ethanol (EtOH), $NH_3 \cdot H_2O$ (13.4 $mol \cdot L^{-1}$), concentrated hydrochloric acid (HCl, 37% (w/w)) and stearic acid were purchased from Kelong Chemical Reagents Factory. The water was deionized. All chemicals were used without further purification.

1.2 Preparation of SiO_2 sols

The SiO_2 sols were prepared by a modified classic Stber method using MTES and TEOS as co-

precursors and ammonia as catalyst. These reagents were successively added into a glass bottle. n_{Si} (total amount of MTES and TEOS):n_{H_2O}:n_{EtOH}:n_{NH_3} was 1:3.25:37.6:0.17 finally. And the molar ratio of MTES/TEOS was 0.3 for the coating with a refractive index of 1.15. The concentration of equivalent SiO_2 was 3% (*w*/*w*) (assuming that 1 mol of TEOS (or MTES) gives 1 mol of SiO_2). The solution was stirred at 30 ℃ for 2 h, and then aged at room temperature for 10 days. Before deposition, the sols were diluted with equal amount of anhydrous ethanol.

1.3 Preparation of TiO_2 sols

TiO_2 sol was prepared by mixing EtOH, H_2O and HCl, followed by dropwise adding *n*-BuTi under stirring. The molar ratio of $n_{n\text{-BuTi}}$:n_{H_2O}:$n_{C_2H_5OH}$:n_{HCl} was 1:3.55:49.75:0.22. The solution was stirred in a closed glass container at 30 ℃ for 2 h, and then aged at room temperature for 7 days. Before deposition, the sols were diluted with anhydrous ethanol, and the final concentration of TiO_2 was 0.75% (*w*/*w*) (assuming that 1 mol of n-BuTi gives 1 mol of TiO_2).

1.4 Films preparation

BK-7 substrates (Φ=35 mm, *d*=3 mm) were cleaned by ultrasonication in acetone for 10 min and wiped carefully before dip-coating. The SiO_2 and TiO_2 sols were deposited on the well-cleaned substrates successively under ambient condition of 30% RH (relative humidity) and 25 ℃. Approximately an interval of 2 minutes was needed to ensure complete evaporation of solvent. The thicknesses of the films were tuned by changing the withdrawal rates. The obtained SiO_2& amorphous-TiO_2 films were labelled as S*x*-AT*y*, where S*x* represents the withdrawal rate applied on SiO_2 layer was *x* and T*y* represents the withdrawal rate applied on TiO_2 layer was *y*. A denotes the amorphous state of TiO_2 nanoparticles. S*x*-CT*y* represents the SiO_2 &TiO_2 films with crystallized anatase TiO_2 and the S*x*-CT*y* films were prepared by heat-treated the S*x*-AT*y* films at 100 ℃ for 1 h and then 400 ℃ for 2 h.

1.5 Characterizations

The surface topography of the coatings was studied with atomic force microscopy (AFM, SEIKO SPA-400, Japan). The surface root-mean-square (RMS) roughness values were obtained from the analysis of atomic force microscopy (AFM) images. Images of sol particles were obtained by the transmission electron microscope (TEM, JEM-100CX, JEOL) with an acceleration voltage of 200 kV. Cross-sections and top-view morphologies of the coatings were investigated by scanning electrons microscope (SEM, Hitachi S-4800, Japan) with an accelerating voltage of 3 kV. The transmittance spectra were measured with an UV-Vis spectrophotometer (Mapada, UV-3100PC, China) over the range of 400~800 nm. The refractive indices and thicknesses of the coatings were determined by an ellipsometer (SENTECH SE850, Germany). The crystallinity of the TiO_2 powders was estimated using an X-ray diffractometer (XRD, Philips X′PertMRD, Netherlands) that was operated at 40 kV and 35 mA with Cu *K*α radiation (λ=0.154 2 nm) in the 2θ range between 20° and 80°. Raman spectra of the TiO_2 films coated on glasses were recorded on a Raman spectrometer (Horiba LabRAM HR, Japan) with an excitation wavelength of 532 nm. The nitrogen adsorption-desorption isotherms of the SiO_2 xerogels were detected on a BET equipment (Autosorb SI, Quanachrome, USA) and the multi-point BET method was applied to determine the pore size distribution and surface area. To determine particle size and distribution, the SiO_2 and TiO_2 sols were analyzed by dynamic light scattering (DLS, Malvern Nano-ZS, England, wavelength of 632.8 nm) at 25 ℃. The chemical binding states and compositions of titania films were measured by XPS (kratos, AXIS Ultra DLD, England) using a monochromatized Al *K*α (1 486.6 eV) X-ray source under ultra-high vacuum (UHV) of 1.33×10^{-6}~1.33×10^{-8} Pa. For determination of the photocatalytic activity, stearic acid was deposited on the samples by dip-coating of a 50 $mmol\cdot L^{-1}$ solution in ethanol at 180 $mm\cdot min^{-1}$ withdrawal rate. After drying at room temperature, the stearic acid coated samples were then directly irradiated with UV light at ambient atmosphere. UV irradiation was provided by a UV reactor with high pressure mercury lamp (250 W) as light source and circulating-water to remove the effect of heat. The photocatalytic decomposition of stearic acid was

monitored by periodic FTIR (Bruker, Tensor 27, Germany) in transmission mode.

2 Results and discussion

2.1 Surface morphology of the SiO_2&amorphous-TiO_2 films

The SiO_2 sols were prepared by a modified classic Stöber method[16] using MTES and TEOS as co-precursors. As our group previously reported[17], these base-catalysed silica particles randomly stack on the substrates; the inter-particle and particle interior mesopores result in the coating with a low refractive index. The incorporation of methyl groups in the MTES enlarges the pore size in the silica particles. The refractive index of the SiO_2 coatings ranged from 1.22 to 1.10 by varying the molar ratio of MTES to TEOS (Fig.S1). The SiO_2 film with the refractive index of 1.15 was selected as the bottom layer.

The top-view SEM image of the bottom SiO_2 coating is shown in Fig.1a. The SiO_2 coating exhibits a porous structure just like a honeycomb. The N_2 sorption-desorption isotherms of SiO_2 xerogels are a type Ⅳ isotherm, typical of mesoporous solids. The pore size of the SiO_2 xerogels is determined to be ~3 nm. And the SiO_2 xerogels has a large specific surface area of 747 $m^2 \cdot g^{-1}$ (Fig.S2). The large surface areas of the mesoporous SiO_2 layer will favour the dispersion of TiO_2 nanoparticles.

The SiO_2 particles were monodisperse with size of *ca.* 17.11 nm, verified by the TEM image and the size analyses (Fig.1(b,f)). Under the acidic conditions, TiO_2 tends to form linear chain network composed mostly of small primary particles[18]. The TiO_2 particles have a much smaller size of *ca.* 2.99 nm (Fig.1f). The TEM image of the TiO_2 nanoparticles is not shown as single TiO_2 particle cannot be seen due to conglomeration. From the XRD pattern (Fig.1c) and Raman spectrum (Fig.S3) of the as-prepared TiO_2 sample without heat-treatment, no peak was observed, which proves that it is amorphous. After depositing the limited small-sized amorphous TiO_2 particles, the loose porous structure disappeared, as shown in SEM image of S140-AT100 in Fig.1d. Meanwhile, from the cross-section SEM images (Fig.1e), it could be seen that the thickness

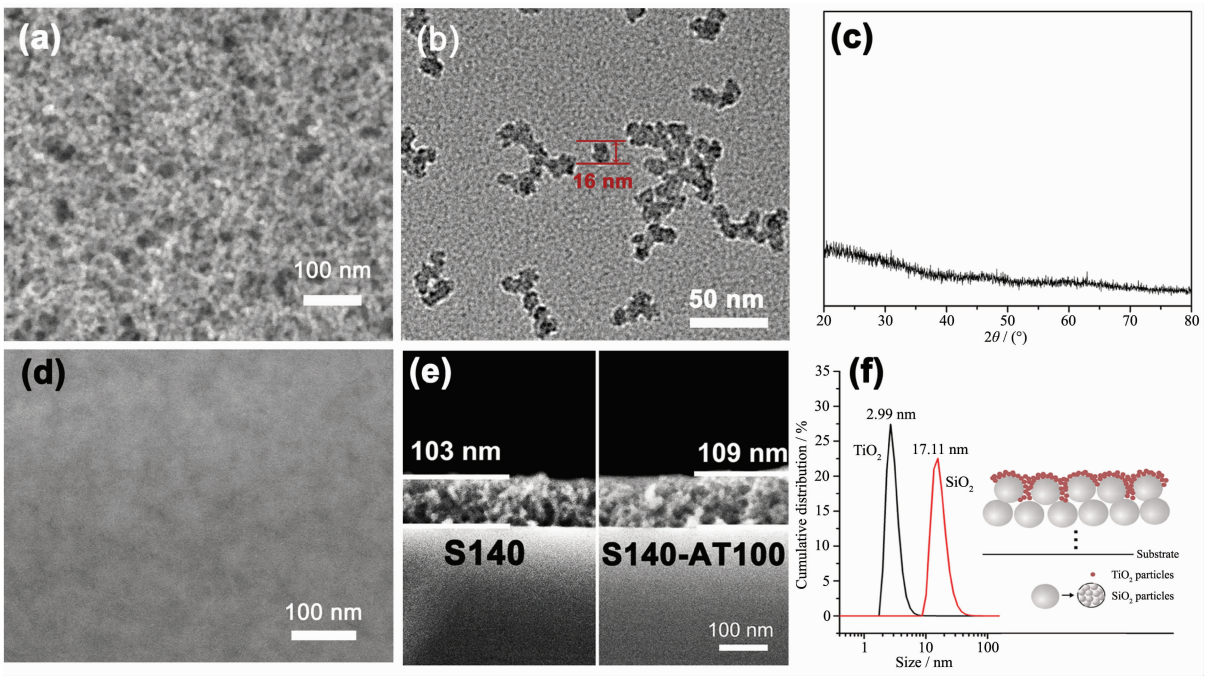

Fig.1 (a) Top-view SEM image of S140; (b) TEM image of the SiO_2 sol; (c) XRD patterns of TiO_2 powders obtained by natural evaporation at room temperature; (d) Top-view SEM image of S140-AT100; (e) Cross-section SEM image of S140 and S140-AT100; (f) Size distribution of SiO_2 and TiO_2 nanoparticles, and schematic illustration of the SiO_2&amorphous-TiO_2 films

value of the S140 and S140-AT100 films are very close, estimated to be *ca.* 103 and 109 nm, respectively, and no distinct boundary between mesoporous SiO_2 layer and TiO_2 nanoparticles can be seen in the S140-AT100 films. These phenomena indicate that the TiO_2 nanoparticles were dispersed well on the SiO_2 support and not enough to form a dense layer with a sufficient thickness.

Fig.2 shows the 3D-AFM images for S140 (Fig. 2a), S140-AT60 (Fig.2b), S140-AT100 (Fig.2c) and AT100 (Fig.2d) films. Fig.2a shows that the SiO_2 film appears as a coarse surface with numerous surface protuberances, several nanometers high and bamboo shoot-shaped. The root-mean-square (RMS) roughness (R_q) value of the S140 film was 2.37 nm. After depositing TiO_2 particles on the porous SiO_2 film, the SiO_2&amorphous-TiO_2 composite films became flat (Fig.2(b,c)) and the R_q value of the S140-AT60 and S140-AT100 coatings decreased to 1.31 and 1.29, respectively. It could be seen as the small TiO_2 nanoparticles filled into the porous SiO_2 matrix and flatted the coarse SiO_2 surface. But due to the limited quantity and the much smaller size of TiO_2 particles compared to SiO_2 particles, the S140-AT60 and S140-AT100 films still presented a coarse surface and the bamboo shoot-shaped protuberances were still visible in the 3D-AFM images. In contrast, the AT100 film (Fig.2d) was very smooth with an R_q value of 0.75 nm, and this smooth and flat surface resulted from the tightly packed TiO_2 nanoparticles. From the AFM and SEM analyses, it can be concluded that the large surface areas of the bottom SiO_2 layer favor the dispersion of TiO_2 nanoparticles, enabling the limited and small-sized TiO_2 nanoparticles to be dispersed effectively instead of forming a dense layer.

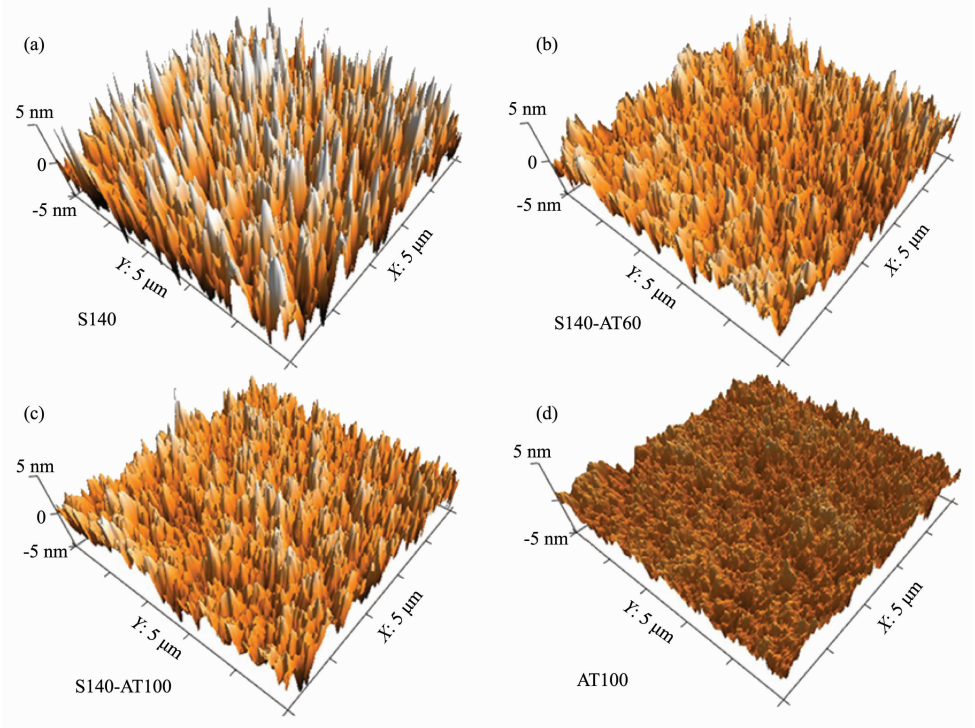

Fig.2　3D-AFM images of S140 (a), S140-AT60 (b), S140-AT100 (c) and AT100 (d) films

2.2　Optical performance of the SiO_2&amorphous -TiO_2 films

The SiO_2&amorphous-TiO_2 films were optimized by adjusting the refractive index and thickness of the SiO_2 layer, or altering the thickness of the TiO_2 layer. The SiO_2 film with the refractive index of 1.15 was selected as bottom layer, as in the preliminary experiments, it matchswell with the TiO_2 nanoparticles and exhibit a better optical performance. The thicknesses of the films were optimized by changing the withdrawal rates. The relative content of the SiO_2 and TiO_2 can be assessed by the thickness of the monolayer

SiO_2 and TiO_2 coatings. The thicknesses of the monolayer of S140, AT60, AT100 and AT140 were measured to be 101, 13, 16 and 21 nm, respectively. The transmission spectra of the resultant SiO_2&amorphous-TiO_2 films coated BK-7 glass are shown in Fig.3. These SiO_2&amorphous-TiO_2 films exhibit a similar AR function with the ideal single-layer AR coatings. The maximum transmittances of S140-AT100 and S140-AT140 coated BK-7 glasses both reached as high as 99.97%, and the S140-AT100 coated glasses had the highest average transmittance of 99.91% in the range of 400~800 nm, enhanced greatly compared to that of blank BK-7 glasses (91.8%).

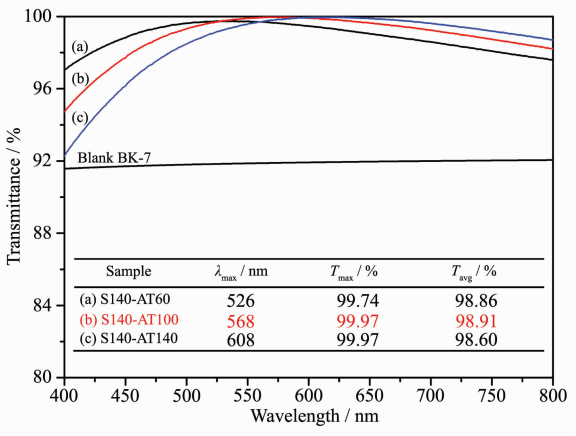

Sample	λ_{max} / nm	T_{max} / %	T_{avg} / %
(a) S140-AT60	526	99.74	98.86
(b) S140-AT100	568	99.97	98.91
(c) S140-AT140	608	99.97	98.60

Inset: Central wavelength (λ_{max}), maximum transmittance (T_{max}) and average transmittance (T_{avg}) of the SiO_2&amorphous-TiO_2 films

Fig.3 Transmission spectra of the SiO_2&amorphous-TiO_2 films coated BK-7 glasses compared with the blank BK-7 glass in the range of 400~800 nm

2.3 Photocatalytic activity

The photocatalytic activities of the SiO_2&TiO_2 coatings were evaluated by the decomposition of stearic acid under UV illumination. Stearic acid can readily form a homogeneous layer onto the surface of the as-prepared coatings. By monitoring the FTIR spectra of stearic acid during UV illumination, the decomposition of stearic acid can be measured.

Fig.4a shows the evolution of the FTIR spectra of the CH_2 groups of stearic acid coated S140-AT100 under UV-illumination, the bands at 2 916 and 2 848 cm^{-1} stemming from the symmetric and asymmetric C-H stretching of CH_2, respectively. The absorbances of the CH_2 bands greatly decreased at the first 10 min. Then the absorption peaks gradually weaken and nearly completely disappeared after 40 min UV-irradiation. It can be concluded that the SiO_2&TiO_2 coating exhibits efficient degradation for stearic acid under UV illumination, suggesting that this nanocomposite film is an effective photocatalyst.

The photodegradation experiments were also carried out on S140-AT60, S140-CT100, AT100 and SiO_2 coatings. The anatase-type TiO_2 were obtained by annealing amorphous TiO_2 at 400 ℃. The crystal forms of the anatase TiO_2 were verified by XRD analyses (Fig.4b) and Raman spectra (Fig.S3). The XRD peaks agreed well with the standard anatase TiO_2 (PDF No. 21-1272). The decreases in absorbances at 2 916 cm^{-1} versus irradiation time are shown in Fig.4c for all samples (The evolutions of IR spectra for all the samples are shown in Fig.S4). A and A_0 are the absorbance at 2 916 cm^{-1} after the UV irradiation and that from the initial surface, respectively. In the case of SiO_2 coating, no significant change in FTIR absorbance was observed after 80 min of UV-irradiation,

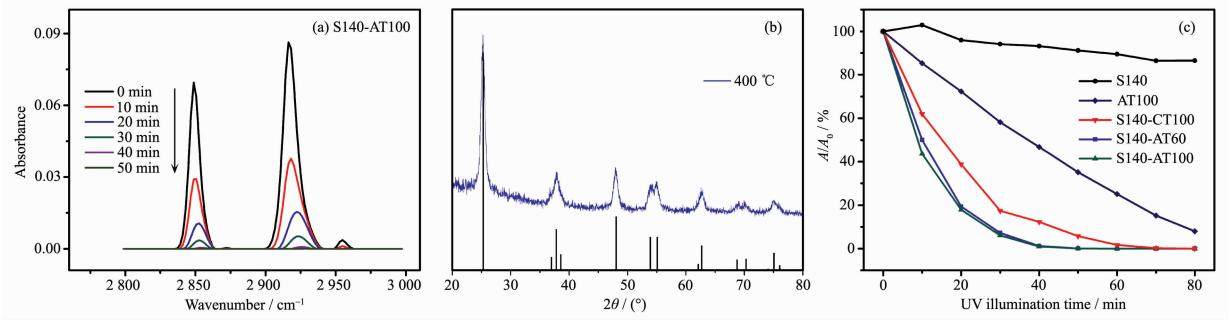

Fig.4 (a) Evolution of FTIR spectra of stearic acid coated S140-AT100 film with UV illumination; (b) XRD patterns of TiO_2 powders heat-treated at 400 ℃ compared with standard anatase TiO_2 in PDF No.21-1272; (c) Absorbance ratio (A/A_0) as a function of UV irradiation time for stearic acid coated samples

indicating that stearic acid decomposition arose exclusively from the photocatalytic activity of the TiO_2 particles. Compared the films with mesoporous SiO_2 as matrix (*i.e.* S140-AT*x* coatings), the monolayer TiO_2 film (AT100) shows a much weaker photocatalytic activity. This superior photocatalytic activity of the S140-AT*x* films can be ascribed to the efficient dispersion of the TiO_2 particles in a very accessible mesoporous matrix, which can greatly enhance the surface areas of TiO_2 particles. It is known that an increase in surface area can facilitate the formation of more effective adsorption sites, which might promote the photocatalytic activity by increasing the concentration of contaminants and reaction intermediates near the TiO_2 surface[19]. More inspiringly, the S140-AT100 films show a higher photocatalytical activity compared to its counterpart with anatase phase, *i.e.* S140-CT100.

2.4 Structure-photocatalytic activity correlations

Inspired by the outstanding activity of S140-AT100, chemical properties of these films were investigated to disclose the correlations between structure and performance. The XPS analyses were conducted on amorphous and anatase titania, respectively. The XPS survey spectra confirms that the as-deposited films are composed of Ti, O, and residual C (Fig.S5). The high resolution XPS spectra of Ti2*p* and O1*s* are shown in Fig.5. As can be seen in Fig.5a, the binding energy difference between the two peaks Ti2$p_{3/2}$ and Ti2$p_{1/2}$ (at 458.7 and 464.4 eV for amorphous titania, and at 458.4 and 464.1 eV for anatase) is always 5.7 eV, corresponding to the spin-orbit coupling of Ti(Ⅳ) chemical state[19].

Fig.5b shows the high resolution XPS spectra of the O1*s* core level. The O1*s* spectra were resolved into two peaks. The peaks at 529.4 eV for amorphous TiO_2 and 529.9 eV for anatase were assigned to surface Ti-O_s[20-21]. The other O1*s* peak respectively located at 530.7 and 529.9 eV for amorphous and anatases titania corresponded to surface hydroxyl groups (-OH_s)[22-23]. The peaks of amorphous titania slightly red-shifted relative to those of anatase titania, which may be ascribed to the difference of binding energy surrounding by the different chemical states of amorphous and anatase titania samples.

The peaks fitting parameters, such as binding energies, peak areas and the calculated atom ratios, are listed in Table 1. The molar ratio of Ti-O_s to Ti are both ~2 (listed in Table 1), calculated from the integrated areas of Ti2*p* and O1*s* at 529.4 eV or 529.9 eV (*i.e.* Ti-O_s) XPS peaks divided by their corresponding sensitivity factors (Ti2*p*=2.001, O1*s*=0.780). However, the amorphous titania show a much higher content of surface hydroxyl groups than anatase sample, and the molar ratios of -OH_s to Ti are 1.12 and 0.53 for amorphous and anatase titania, respectively. The abundant surface hydroxyl groups have a great effect on photocatalytic activity.

The widely accepted photoactivation mechanism is as follows: When a TiO_2 photocatalyst absorbs a photon with energy equal to or greater than its band-gap, electrons are excited from the valence band to the conduction band; subsequently, the photogenerated electrons (e) and holes (h) migrate to the surface

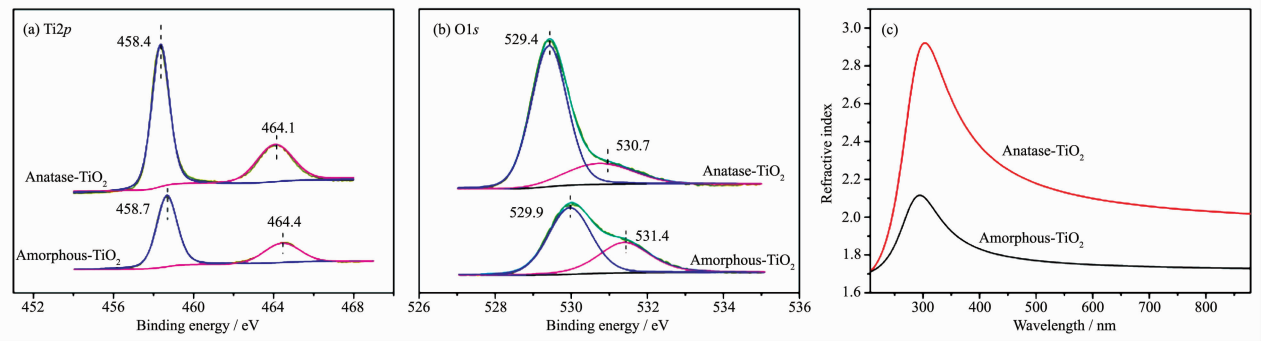

Fig.5 XPS spectra of Ti2*p* (a) and O1*s* (b) of amorphous and anatase TiO_2 samples; (c) dispersion curve of amorphous and anatase TiO_2 films

Table 1 Peaks fitting parameters for the O1*s* and Ti2*p* regions of amorphous and anatase titania

Sample	Ti peak area	O peak area (Ti-O_s)	O peak area (-OH_s)	$n_{Ti\text{-}O_s}/n_{Ti}$	$n_{\text{-}OH_s}/n_{Ti}$
Amorphous-titania	83 603	63 510	36 826	1.94	1.12
Anatase-titania	150 166	115 607	31 006	1.97	0.53

of the photocatalyst and are trapped there. The trapped electron and hole react with acceptor (*e.g.*, O_2) or donor molecules (*e.g.*, RH), respectively, or recombine at surface trapping sites[24]. The photocatalytic reactions kinetics of TiO_2 depend on both the amount of substrates adsorbed on the surface to be reduced or oxidized by photoexcited electron (e^-) or positive hole (h^+), respectively, and rate of the recombination of e^- and h^+[25].

Surface Ti-OH groups play an important role in trapping charge carriers, which is needed in the photocatalysis process to suppress recombination and increase the probability of interfacial charge transfer. The Ti-OH groups trap electron and hole forming Ti^{3+}-OH groups and Ti^{4+}-·OH radicals, respectively. The role of the Ti-OH groups trapping hole was disputed by some researcher [12], but the contribution of surface Ti-OH groups to electron trapping has been verified experimentally and theoretically[26]. Meanwhile, the surface OH groups can protect the recombination of the excited carriers from the defective states by compensate the dangling bonds at defects and thus prolong the lifetime of the photoexcited carrier[13,27].

In addition, the refractive index of the amorphous and anatase TiO_2 are 1.74 and 2.10 at 632.8 nm, respectively (Fig.5c), indicating the prepared amorphous TiO_2 films possessing a relative loose structure compared with the anatase films. The loose structure can lead to a faster migration of the photoexcited electrons and holes from the internal to surface and better photocatalytic activity[28].

These differences between amorphous and anatase TiO_2 mainly result from the further condensation between the surface -OH groups[29], and the films shrinkage and crystallization during the heat treatment process. In a word, the amorphous TiO_2 nanoparticles featured abundant hydroxyl groups and loose structure. These characters may be preferable to crystal structure for enhancing photocatalytic activity. Thus the S*x*-AT*y* films exhibit a slight higher photocatalytic decomposition rate compared to S*x*-CT*y* films.

3 Conclusions

In summary, this article presents a simple and facile method to enhance the photocatalytic activity of amorphous TiO_2 by dispersion of amorphous TiO_2 nanoparticles onto a mesoporous SiO_2 coating. This structure greatly increased the surface areas of the TiO_2 particles and the SiO_2&amorphous-TiO_2 films exhibit an enhanced photocatalytic activity than the monolayer amorphous TiO_2 film. The SiO_2&amorphous-TiO_2 even exhibit a higher photocatalytic activity than the counterparts with anatase phase. This higher photocatalytic activity is attributed to abundant surface hydroxyl groups and relative loose structure of the amorphous TiO_2 nanoparticles, which can help enhance photocatalytic activity through reducing recombination of electron-hole pairs and increasing the migration rates of the photoexcited electrons and holes, respectively. The SiO_2&amorphous-TiO_2 films also exhibit excellent AR properties. These AR films with efficient photocatalytic activity can find potential applications in energy-related instruments and optical devices.

Supporting information is available at http://www.wjhxxb.cn

References:

[1] Zhang X T, Sato O, Taguchi M, et al. *Chem. Mater.*, **2005**, **17**:696-700

[2] Faustini M, Grenier A, Naudin G, et al. *Nanoscale*, **2015**,**7**: 19419-19425

[3] HU Teng (胡腾), YE Long-Qiang (叶龙强), LI Wen-ling (李文玲), et al. *Chinese J. Inorg. Chem.*(无机化学学报), **2014**, **30**:1778-1782

[4] Miao L, Su L F, Tanemura S, et al. *Appl. Energy*, **2013**,**112**:

1198-1205

[5] Lin W S, Zheng J X, Yan L H, et al. *Results Phys*., **2018**,**8**: 532-536

[6] Li X Y, He J H. *ACS Appl. Mater. Interfaces*, **2013**,**5**:5282-5290

[7] Yao L, He J H, Geng Z, et al. *Nanoscale*, **2015**,**7**:13125-13134

[8] Guldin S, Kohn P, Stefik M, et al. *Nano Lett.*, **2013**,**13**:5329-5335

[9] Tanaka K, Capule M F V, Hisanaga T. *Chem. Phys. Lett.*, **1991**,**187**:73-76

[10]Nakamura M, Aoki T, Hatanaka Y, et al. *J. Mater. Res.*, **2011**,**16**:621-626

[11]Li Y, Sasaki T, Shimizu Y, et al. *J. Am. Chem. Soc.*, **2008**, **130**:14755-14762

[12]Nakamura R, Ohashi N, Imanishi A, et al. *J. Phys. Chem. B*, **2005**,**109**:1648-1651

[13]Nakamura M, Kato S, Aoki T, et al. *J. Appl. Phys.*, **2001**,**90**: 3391-3395

[14]Sun Z G, Li X S, Zhu X, et al. *Chem. Vap. Deposition*, **2014**, **20**:8-13

[15]Huang J, Liu Y Y, Lu L F, et al. *Res. Chem. Intermed.*, **2011**,**38**:487-498

[16]Stber W, Fink A, Bohn E. *J. Colloid Interface Sci.*, **1968**,**26**: 62-69

[17]Zhang Y L, Zhao C X, Wang P M, et al. *Chem. Commun.*, **2014**,**50**:13813-13816

[18]Vincent A, Babu S, Brinley E, et al. *J. Phys. Chem. C*, **2007**,**111**:8291-8298

[19]Qi K H, Chen X Q, Liu Y Y, et al. *J. Mater. Chem.*, **2007**, **17**:3504-3508

[20]Song Z, Hrbek J, Osgood R. *Nano Lett.*, **2005**,**5**:1327-1332

[21]Dupin J C, Gonbeau D, Vinatier P, et al. *Phys. Chem. Chem. Phys.*, **2000**,**2**:1319-1324

[22]Pouilleau J, Devilliers D, Groult H, et al. *J. Mater. Sci.*, **1997**,**32**:5645-5651

[23]Yu J G, Zhao X J, Zhao Q N. *Thin Solid Films*, **2000**,**379**:7-14

[24]Fujishima A, Zhang X, Tryk D. *Surf. Sci. Rep.*, **2008**,**63**:515-582

[25]Ohtani B, Ogawa Y, Nishimoto S. *J. Phys. Chem. B*, **1997**, **101**:3746-3752

[26]Szczepankiewicz S H, Colussi A J, Hoffmann M R. *J. Phys. Chem. B*, **2000**,**104**:9842-9850

[27]Hatanakaa Y, Naitob H, Itouc S, et al. *Appl. Surf. Sci.*, **2005**,**244**:554-557

[28]Ren L, Li Y Z, Hou J T, et al. *ACS Appl. Mater. Interfaces*, **2014**,**6**:1608-1615

[29]Gao Y F, Masuda Y, Koumoto K. *Langmuir*, **2004**,**20**(8):3188-3194